

Document downloaded from:

<http://hdl.handle.net/10251/83593>

This paper must be cited as:

Martín García, N.; Li, Z.; Martínez Triguero, L.J.; Yu, J.; Moliner Marin, M.; Corma Canós, A. (2016). Nanocrystalline SSZ-39 zeolite as an efficient catalyst for the methanol-to-olefin (MTO) process. *Chemical Communications*. 52(36):6072-6075. doi:10.1039/C5CC09719C



The final publication is available at

<http://doi.org/10.1039/c5cc09719c>

Copyright Royal Society of Chemistry

Additional Information

**Nanocrystalline SSZ-39 zeolite as efficient catalyst for the Methanol-to-Olefins (MTO)
process**

Nuria Martín,⁺ Zhibin Li,⁺ Joaquín Martínez-Triguero, Manuel Moliner,^{*} Avelino
Corma^{*}

Instituto de Tecnología Química (UPV-CSIC), Universidad Politécnica de Valencia,
Consejo Superior de Investigaciones Científicas, Valencia, 46022, Spain

⁺ These authors contributed equally to this work.

^{*}Corresponding authors: E-mail addresses: acorma@itq.upv.es; mmoliner@itq.upv.es

1.- Introduction

Light olefins, such as ethylene and propylene, are mainly obtained from fluid catalytic cracking [1-3] and from steam cracking of hydrocarbons, preferentially LPG and naphtha.[4, 5] However, in the last years, since methanol can be efficiently obtained from different non-petroleum based feedstocks, such as coal or natural gas, the production of these light olefins from methanol through the so-called methanol-to-olefins (MTO) process, has been notoriously increased.[6-8]

One of the commercial catalysts for the MTO reaction is the SAPO-34, which is the silicoaluminophosphate form of the CHA material.[9, 10] The excellent catalytic behavior of the SAPO-34 for the MTO process could be mainly explained by its crystalline structure, combining the presence of large cavities and small pores.[8, 11] Indeed, the large cavities allow the formation of the required large “hydrocarbon pool” intermediates to produce the light olefins,[12, 13] and the small pores favor the diffusion of the desired linear light olefins versus aromatic or branched molecules.

However, the formation of these large organic species within the large cavities (“hydrocarbon pool”) combined with severe mass transfer restrictions, may result in a fast deactivation of the MTO catalyst by coke formation and low catalyst utilization.[14] Thus, to achieve mass transfer rate enhancement will be a key objective when designing new small pore zeolite-based MTO catalysts to increase catalytic activity and catalyst lifetime.[15, 16] In this sense, the generation of intra-crystalline mesoporosity,[17-23] or the reduction of the crystal size to the nanometer scale,[24-26] has allowed increasing the catalytic properties of the SAPO-34.

Besides SAPO-34, the silicoaluminate form of CHA, SSZ-13, has also been described as a very efficient catalyst for the MTO reaction.[27-30] This was especially so when some mesoporosity was generated in the zeolite crystals, or the zeolite was synthesized in the form of very small crystal sizes.[31, 32] It is worth noting that, in general, the hydrothermal stability and Brönsted acidity of silicoaluminate materials are much higher than those of their silicoaluminophosphate counterparts, especially at low and moderate temperatures.[33, 34] Therefore, the design of silicoaluminate materials with the adequate physico-chemical properties for the MTO reaction is a matter of interest to prepare new commercial catalysts for the MTO process.

When considering other potential zeolites as catalysts for MTO, SSZ-39 is a silicoaluminate material with the AEI structure that, as chabazite, shows the presence of large cavities within its crystalline framework interconnected through small pore openings.[35, 36] Despite the structural similarities between CHA and AEI frameworks, there are very few reports using SSZ-39 zeolite as catalyst for the MTO reaction.[37] Perhaps the small range for synthesis conditions to crystallize SSZ-39 materials could explain the small number of reports on this zeolite as MTO catalysts.[35, 38, 39] Indeed, with the former synthesis procedure, SSZ-39 material can only be synthesized under very restricted Si/Al ratios (~ 8), very low solid yields (below 50%), and relative large crystal sizes (0.5-1 μm).[35, 38, 39]

Nevertheless, the synthesis of the SSZ-39 has been remarkably improved in the last years following zeolite-to-zeolite transformations, using high-silica FAU zeolites as silicon and aluminum precursor, and tetraethylphosphonium (TEP) [40, 41] or N,N-dimethyl-3,5-dimethylpiperidinium (DMP) [42] as organic structure directing agents (OSDAs). These novel synthesis methodologies allow improving the solid yields up to 90%, and the Si/Al ratios of the synthesized materials up to 16,[41] [42] but the reported crystal sizes are similar to the ones described for the original SSZ-39 material (0.5-1 μm).[40, 41] However, the preparation of the SSZ-39 material in nanosized form would be of much interest for the application of this zeolite for the MTO process.

Taking as objective to decrease the crystal size of the SSZ-39 material, it would be required to accelerate the nucleation step during its hydrothermal synthesis. Taking this into account, we have made the hypothesis that the use of FAU zeolite as zeolitic precursor under the adequate synthesis conditions, could increase the rate of formation of the SSZ-39-precursor nuclei, since both zeolitic materials present common small structural building units within their structures, as the double-six member rings (D6Rs). Therefore, if faster nucleation rates are achieved during the synthesis of the SSZ-39 material, samples with smaller crystallite size could be obtained.

Herein, we present the preparation of the SSZ-39 zeolite with nanosized crystals of 40-50 nm, which have been synthesized following a zeolite-to-zeolite transformation procedure, using high-silica FAU as silicon and aluminum source and TEP as OSDA. This nanosized SSZ-39 material shows excellent catalytic properties for the MTO reaction,

including a remarkable longer lifetime than standard SSZ-13 and SSZ-39 materials. The nanosized SSZ-39 crystals allow improving the diffusion rate of the reactants and products involved in the MTO reaction, and notoriously decrease the negative effect of coke deposition within the zeolitic cavities.

2.- Experimental Section

2.1.- Zeolite syntheses

2.1.1- Synthesis of standard SSZ-13

N,N,N-trimethyl-1-adamantonium (TMAda): 29.6 g of 1-Adamantamine (Sigma-Aldrich) and 64 g of potassium carbonate (Sigma-Aldrich) were mixed with 320 ml of chloroform. At this point, 75 g of methyl iodide was added dropwise while the reaction was stirred in an ice bath. The reaction was maintained during 5 days under agitation at room temperature. The mixture was filtered and washed with diethyl ether, and the resultant solid further extracted with chloroform. The final product was N,N,N-trimethyl-1-adamantammonium iodide. This iodide salt was anion exchanged using an ion exchange resin achieving the hydroxide form.

SSZ-13 zeolite: Conventional SSZ-13 was synthesized with the following gel composition: 0.1 Na₂O : 1 SiO₂ : 0.025 Al₂O₃ : 0.2 TMAdaOH : 44 H₂O. TMAdaOH was firstly mixed with NaOH and deionized water at room temperature until it was completely dissolved. Then, SiO₂ (Aerosil) was added to the TMAdaOH solution. Finally, Al₂O₃ was dissolved into the solution mentioned above, and the resulting gel was stirred at room temperature for 1 hour to obtain a homogeneous gel. The gel was transferred into a Teflon-lined steel autoclave and kept statically in an oven at 160°C for 6 days. The product was separated by filtration, washed with deionized water and dried at 100°C. The catalyst was calcined in air at 580°C to remove the template. H-SSZ-13 was obtained by ion exchange of calcined sample with 2.5 M NH₄Cl solution (80°C and liquid to solid ratio of 10) for 2 hours. Finally, the NH₄-exchanged material was calcined at 500 °C for three hours in air.

2.1.2- Synthesis of N-SSZ-39

N,N-dimethyl-3,5-dimethylpiperidinium (DMP): 10 g of 3,5-dimethylpiperidine (C₇H₁₅, Acros Organics, 96%, cis-trans mixture) was mixed with 140 ml of methanol (CH₃OH, Scharlab, 99.9%) and 19.51 g of potassium carbonate (KHCO₃, Sigma Aldrich, 99.7%). 54 g of methyl iodide (CH₃I, Sigma Aldrich, 99.9%) was added dropwise, and the

resultant mixture maintained under stirring for 7 days. After this time, MeOH was partially removed under vacuum, and the iodide salt was precipitated by addition of diethyl ether. For its use in the synthesis of zeolites, the final product was ion exchanged to the hydroxide form using a commercially available hydroxide ion exchange resin (Dowex SBR).

N-SSZ-39 zeolite: First, the aqueous solution of N,N-dimethyl-3,5-dimethylpiperidinium (DMP) hydroxide was mixed with a 20%wt aqueous solution of sodium hydroxide (NaOH granulated, Scharlab). Then, the crystals of USY zeolite (CBV-720 with $\text{SiO}_2/\text{Al}_2\text{O}_3=21$) were introduced in the above solution, and the resultant mixture was stirred until complete homogenization. The chemical composition of the synthesis gel was $\text{SiO}_2 : 0.045 \text{ Al}_2\text{O}_3 : 0.2 \text{ NaOH} : 0.2 \text{ DMP} : 15 \text{ H}_2\text{O}$. The gel was transferred into a stainless steel autoclave with a Teflon liner. The crystallization was then conducted at 135°C for 7 days under static conditions. The solid product was filtered, washed with water and dried at 100°C. The sample was calcined in air at 550°C for 4h. The acid form of the N-SSZ-39 material was obtained by ion exchange of the calcined sample with 2.5 M NH_4Cl solution (80°C and liquid to solid ratio of 10) for 2 hours. Finally, the NH_4 -exchanged sample was calcined at 500 °C for three hours in air.

2.1.3- Synthesis of P-SSZ-39

First, the aqueous solution of tetraethylphosphonium (TEP) hydroxide was mixed with a 20%wt aqueous solution of sodium hydroxide (NaOH granulated, Scharlab). Then, the crystals of USY zeolite (CBV-720 with $\text{SiO}_2/\text{Al}_2\text{O}_3=21$) were introduced in the above solution, and the resultant mixture was stirred until complete homogenization. The chemical composition of the synthesis gel was $\text{SiO}_2 : 0.045 \text{ Al}_2\text{O}_3 : 0.1 \text{ NaOH} : 0.2 \text{ TEP} : 5 \text{ H}_2\text{O}$. The crystallization was conducted at 150°C for 9 days under static conditions. The solid product was filtered, washed with water and dried at 100°C. The sample was calcined under a hydrogen atmosphere at 800°C for 4h to assure the complete decomposition of the phosphorous-containing species, followed by another calcination in air at 550°C for 2 hours. The acid form of the P-SSZ-39 material was obtained by ion exchange of the calcined sample with 2.5 M NH_4Cl solution (80°C and liquid to solid ratio of 10) for 2 hours. Finally, the NH_4 -exchanged sample was calcined at 500 °C for three hours in air.

2.2.- Characterization

The crystallinity of the samples was followed by powder X-ray diffraction (PXRD) with a Panalytical CUBIX diffract meter with monochromatic $\text{CuK}_{\alpha 1,2}$ radiation ($\lambda=1.5406, 1.5444 \text{ \AA}$; $\text{K}\alpha_2 / \text{K}\alpha_1$ intensity ratio=0.5). The morphology and particle size of the zeolite were characterized by Scanning Electron Microscope (SEM, JEOL JSM-6300). The MAS NMR spectra were recorded with a Bruker AV400 spectrometer. Solid state ^{27}Al MAS NMR spectra were recorded at 104.218 MHz with a spinning rate of 10 kHz at a 90° pulse length of 0.5 μs with 1 s repetition time. Solid-state ^{31}P NMR spectra were recorded at 161.9 MHz with a spinning rate of 10 kHz, a $\pi/2$ pulse of 5 μs with 20 s repetition time. ^{27}Al and ^{31}P chemical shifts were referred to $\text{Al}(\text{H}_2\text{O})_6$ and H_3PO_4 , respectively. Chemical composition was determined by inductively coupled plasma atomic absorption spectroscopy (ICP-OES) using a Varian 715-ES. The BET surface area, micropore volume and pore volume distribution were measured by N_2 adsorption in a Micromeritics ASAP2000. NH_3 -TPD experiments were carried out in a Micromeritics 2900 apparatus. A calcined sample (100 mg) was activated by heating to 400°C for 2 h in an oxygen flow and for 2 h in argon flow. Subsequently, the samples were cooled down to 176°C , and NH_3 was adsorbed. The NH_3 desorption was monitored with a quadrupole mass spectrometer (Balzers, Thermo Star GSD 300T) while the temperature of the sample was ramped at $10^\circ\text{C min}^{-1}$ in helium flow. Total ammonia adsorption was measured by repeated injection of calibrated amounts of ammonia at 176°C until saturation. Ammonia desorption was recorded by means of the mass 15, since this mass is less affected by the desorbed water.

2.3.- Catalytic experiments

The catalyst was pelletized, crushed and sieved into 0.2-0.4 mm particle size. 50 mg of sample was mixed with 2 g quartz (Fluka) before being introduced into the fixed-bed reactor (7mm diameter). N_2 (30mL/min) was bubbled in methanol hold at -17°C , giving a $\text{WHSV}=0.8 \text{ h}^{-1}$. The catalyst was first activated with a nitrogen flow of 80 ml/min for 1 h at 540°C , and then the temperature was decreased to reaction conditions (350°C). Each experiment was analyzed every 5 minutes with an online gas chromatograph (Bruker 450GC, with PONA and Al_2O_3 -Plot capillary columns, and two FID detectors). After reaction, the catalyst was regenerated at 540°C in 80ml of air for 3h and the reaction was repeated again. Preliminary experiments were carried out at constant

WHSV, different amount of catalyst and increasing flow rates, and later with catalyst with in different particle sizes, to check that, at the selected reaction conditions the process is not controlled by either external or intraparticle diffusion. Conversion and selectivities were considered in carbon basis and methanol and dimethylether were lumped together for calculation of conversion.

3.- Results and discussion

3.1.- Zeolite synthesis and characterization

To synthesize the SSZ-39 material with small crystal sizes, a high-silica FAU zeolite as silicon/aluminum source and two different organic molecules, DMP and TEP, as OSDAs have been studied under different synthesis conditions. In this sense, the presence and concentration of alkali cations in the synthesis media, and the dilution of the gel, are two well-known variables that can influence the size of the zeolitic crystals during the hydrothermal synthesis.[43, 44] Thus, the following molar ratios of NaOH/Si and H₂O/Si, [0.05, 0.1, 0.2] and [5, 15], respectively, have been studied for each OSDA. The remaining synthesis conditions were Si/Al=11 and OSDA/Si=0.2, and the crystallization of the resultant gels were carried out at 135°C (DMP) or 150°C (TEP) for 9 days under static conditions.

The results for each OSDA are summarized in [Figure 1](#). As can be seen there, different SSZ-39 materials can be obtained using the two proposed OSDAs, requiring slightly different synthesis conditions depending on the OSDA (see N-SSZ-39 and P-SSZ-39 in [Figure 1](#)). Under the studied conditions, higher NaOH/Si ratios are required to achieve pure crystalline SSZ-39 materials using the ammonium-based OSDA (NaOH/Si~0.2, see N-SSZ-39 in [Figure 1](#)) than using the phosphonium-based OSDA (NaOH/Si~0.1, see P-SSZ-39 in [Figure 1](#)). It is worth noting that the previously reported SSZ-39 synthesis using TEP as OSDA described by Sano et al. also required a NaOH/Si molar ratio of 0.1.[40, 41]

The PXRD patterns of the N-SSZ-39 and P-SSZ-39 samples reveal the crystallization of the pure AEI structure (see [Figure 2](#)), but the different width and overlapping of the diffraction peaks suggest the presence of different crystal sizes for these two samples of SSZ-39. Indeed, different crystal sizes were measured by scanning electron microscopy (SEM, see [Figure 3](#)). The N-SSZ-39 sample shows homogeneous crystal sizes of 0.2-0.4 μm (see N-SSZ-39 in [Figure 3](#)), while the P-SSZ-39 sample contains

much smaller crystal sizes within the nanoscale range (~40-50 nm, see P-SSZ-39 in Figure 3).

Although the preferential directing effect of the phosphonium-based OSDA to form nanosized SSZ-39 crystals is not fully understood, the stronger interactions of the phosphonium species in the synthesis media with the inorganic species may result in an increase in the ratios of the nucleation/crystallization rates.[44] Additional synthesis and characterization studies are currently being performed to test this hypothesis.

The as-prepared N-SSZ-39 and P-SSZ-39 materials have been calcined in air at 550°C to remove the organic species occluded within the crystalline structures. It is important to note that the P-SSZ-39 material has been first treated under hydrogen atmosphere at 800°C for 4h to favor the decomposition/elimination of most of the phosphorous-containing species. ³¹P MAS NMR spectrum of the as-prepared P-SSZ-39 material shows the presence of a single band centered at ~40 ppm (see P-SSZ-39_a.p. in Figure 4), which is characteristic for phosphonium species, indicating that the entrapped TEP molecules are intact within the AEI structure. Moreover, chemical analysis reveals a P/TO₂ molar ratio of ~0.085, which corresponds to ~1 TEP molecule per cavity.(comprobar) After the thermal treatment with H₂, almost 80-85% of the initial phosphorous has been removed, and the small amount of residual phosphorous species remain as extra-framework phosphate species (see the ³¹P MAS NMR spectrum for the P-SSZ-39_calc material in Figure 4). Finally, the samples have been ammonium exchanged to remove the extra-framework sodium cations, followed by calcination with air at 500°C to generate the acid-form of the SSZ-39 zeolites.

These calcined materials have been characterized by N₂ adsorption to study their textural properties. Both materials show similar BET surface area (~520 m²/g, see Table 1) but, as expected by its lower crystal size, the P-SSZ-39 material presents higher external surface area and lower micropore volume (42 m²/g and 0.23 cm³/g, respectively) than N-SSZ-39 material (15 m²/g and 0.25 cm³/g, respectively, see Table 1).

Chemical analyses of the ammonium-exchanged and calcined SSZ-39 materials, indicate similar Si/Al ratios (~8.5, see Table 1) and the absence of sodium cations in both final solids. The coordination of aluminum atoms within the acid SSZ-39 materials has been studied by solid ²⁷Al MAS NMR spectroscopy. Both acid SSZ-39 materials

show similar ^{27}Al MAS NMR spectra, presenting a main band centered at ~ 55 ppm, a broad shoulder between 45-20 ppm, and finally, a small band centered at $\sim -10-0$ ppm, which have been assigned to tetrahedrally coordinated Al in framework positions, distorted tetrahedrally coordinated Al species in framework positions, and octahedrally coordinated extra-framework aluminum species, [REF] respectively (see N-SSZ-39_Exc and P-SSZ-39_Exc in Figure 5).

The Brönsted acidity of these samples has been measured by means of temperature-programmed desorption (TPD) of ammonia. The acid SSZ-39 materials show similar NH_3 desorption curves, both presenting a maximum desorption band centered between 420-450°C (see N-SSZ-39 and P-SSZ-39 in Figure 6). The quantification of the desorbed ammonia molecules reveals that both SSZ-39 materials show analogous Brönsted acidities (~ 0.5 mmol NH_3/g , see Table 2).

For comparison purposes, a standard SSZ-13 zeolite has also been prepared under conventional synthesis conditions using N,N,N-trimethyladamantammonium (TMAda) cation as OSDA (see synthesis conditions in the experimental section).[45] The PXRD pattern of this material confirms the crystallization of the pure CHA structure (see SSZ-13 in Figure 2), and SEM microscopy indicates that the crystal sizes obtained for the conventional SSZ-13 material ($\sim 1 \times 0.2$ μm , see Figure 3) are larger than those achieved for the SSZ-39 materials (see Figure 3). The textural properties of the SSZ-13 material have been measured by N_2 adsorption, obtaining a BET surface area and a micropore volume of 520 m^2/g and 0.25 cm^3/g , respectively, which are analogous to the values achieved for the acid N-SSZ-39 material (see Table 1). Finally, the acidity of the SSZ-13 material has been measured by NH_3 -TPD. The amount of ammonia desorbed in the SSZ-13 material is lower (~ 0.35 mmol NH_3/g , see Table 2) than the amount desorbed in the SSZ-39 materials (~ 0.50 mmol NH_3/g , see Table 2). The lowest acidity measured for the SSZ-13 material could be mainly attributed to its higher Si/Al ratio (~ 15) compared to SSZ-39 materials (Si/Al ~ 8.5), but the presence of larger diffusion paths within the larger crystal sizes of the SSZ-13 material may also influence the amount of desorbed ammonia.

3.2.- Catalytic activity

The catalytic activity of the SSZ-13 and SSZ-39 materials has been evaluated for the methanol to olefins (MTO) reaction at $WHSV=0.8\text{ h}^{-1}$ and 350°C (see reaction conditions in the experimental section). The initial methanol conversion for the three samples is complete (100%) but, as can be seen in [Figure 7](#), these materials suffer different catalyst deactivation profiles with time-on-stream (TOS). The conventional SSZ-13 material shows the fastest catalyst deactivation with methanol conversion dropping below 50% after 310 min of TOS. In contrast, both SSZ-39 materials, i.e. N-SSZ-39 and P-SSZ-39, show higher catalyst lifetime than the conventional SSZ-13 catalyst, with methanol conversion dropping below 50% after 540 and 940 minutes on stream for N-SSZ-39 and P-SSZ-39, respectively (see [Figure 7](#)).

These different deactivation profiles reveal that the physico-chemical properties of each catalyst are clearly influencing their catalytic behaviour. Indeed, it has been broadly described in the literature that small pore zeolite-based MTO catalysts with excessive Brönsted acidity or mass transfer restrictions within the crystals, suffer from severe catalytic deactivation by coke formation.[6-8] Thus, since the Brönsted acidity measured for the SSZ-13 material is lower than the Brönsted acidity observed for the SSZ-39 materials (see ammonia desorption values in [Table 2](#)), the faster SSZ-13 catalyst deactivation must be mainly attributed to its larger crystal sizes compared to SSZ-39 materials (see [Table 1](#)). In a similar way, the small crystal sizes of the nanosized P-SSZ-39 material would mainly explain its remarkable catalyst lifetime increase compared to N-SSZ-39, since the Brönsted acidities of these two materials are analogous (see [Tables 1 and 2](#)). The different selectivities to products have been compared at constant conversion of methanol (see [Figure 8](#)). This representation could allow detecting particular diffusion restrictions during the catalyst deactivation. However, these three materials show a linear dependence between the different product yields with methanol conversion values (see [Figure 8](#)), indicating that the yields to the different products are not controlled by diffusion during deactivation. In other words, the deactivation of these SSZ-13 and SSZ-39 materials is “non-selective”, and the selectivity to the different products is independent of the coke content. Similar “non-selective” deactivation profiles have been previously reported for ZSM-5,[46] SSZ-13,[47] SAPO-34,[26, 33] and SAPO-18.[48] Moreover, comparing selectivities at constant conversion allows discriminating the influence of thermodynamical

equilibrium of olefins, at 100% conversion of methanol+DME, from the true selectivity of the hydrocarbon pool at lower conversions.[26]

Regarding the product selectivities at different methanol conversion values, it can be clearly seen that the SSZ-13 and SSZ-39 materials show different product distributions (see **Figure 9**). In general, it can be observed that the two SSZ-39 samples provide much higher selectivity to propylene and lower to ethylene than the conventional SSZ-13 material (see **Figure 9**). Indeed, the C2/C3 ratio with TOS is much higher for the SSZ-13 material than for the two SSZ-39 materials (see **Figure 10**). Similar trends for the C2/C3 ratios have also been observed for the AEI and CHA structures in their SAPO forms.[49,50] This different product selectivity could be attributed to the different shape of the zeolitic cages present in both materials, being the AEI cage basket-shaped and wider at the bottom than the CHA cage, which is more symmetric.[37, 49] Thus, the larger size of the AEI cage would allow the formation of aromatic cycles within the “hydrocarbon pool” transient-state with the adequate size to increase the propylene selectivity.[30] In fact, other small pore zeolites, as RUB-13 (RTH), presenting larger cages than those of AEI and CHA, have also shown high selectivity to propylene.[51] However, other parameters in addition to the cage dimensions may be taken into consideration to explain the product selectivity observed for the MTO reaction when using small pore zeolites. In this sense, two hydrocarbon-pool cycles, olefinic and aromatic, influence the product selectivity of the MTO reaction when ZSM-5 is used as catalyst.[54-56] The decrease of the acidity within the ZSM-5 zeolite allows mostly suppressing the aromatic cycle, characterized by a high yield of ethylene, leading to high selectivities to propylene due to the low intrinsic rate constants for obtaining ethylene by methylation-cracking at moderate temperatures as those of MTO. Recently, it has been described for SAPO-18 (AEI) materials that the aromatic-based cycle presents higher energy barriers, explaining the prevalence of the olefin cycle, and therefore, a higher selectivity to propylene.[59, 60]

The values of hydrogen transfer index (HTI, C_3/C_3^-) for the different materials are summarized in **Figure 11**. If the HTI values are compared at constant methanol conversion, it can be seen (**Figure 11-bottom**) that, as occurs for the selectivities to products, two zones are well differentiated. Initially, at 100% methanol conversion, the “initial” hydrogen transfer values are higher due to the formation of the hydrocarbon

pool aromatic species. In fact, the formation of hexamethylbenzene cations implies cyclization and hydrogen transfer to an olefin precursor that desorbs as paraffin (propane). Once the hydrocarbon pool is formed within all the cages, subsequent cyclization on the previously formed monoaromatic species causes their growth and progressive deactivation. These “secondary” hydrogen transfer reactions are lower and appear in a second zone, in which methanol conversion is below 100%. In this sense, the higher “initial” HTI values observed for the SSZ-39 samples could be explained by their higher acidity (see [Table 2](#)), while the higher “secondary” HTI values observed for the SSZ-13, which agrees with the faster catalytic deactivation observed in the methanol reaction, could be mainly attributed to its larger crystal sizes (see [Figure 7](#)). Regarding SSZ-39 materials, the nanosized P-SSZ-39 shows the lowest HTI values (see [Figure 11-bottom](#)), as it could be expected by its smaller crystal sizes.

4.- Conclusions

The synthesis of the nanosized SSZ-39 material has been achieved following a zeolite-to-zeolite transformation methodology, using a high silica FAU zeolite as Si and Al source and tetraethylphosphonium (TEP) cations as OSDAs. The nanosized nature of the SSZ-39 has been confirmed by scanning electron microscopy, observing a homogeneous crystal size distribution of ~40-50 nm. On the other hand, ²⁷Al MAS NMR spectroscopy shows that most of the Al species remain in tetrahedral coordination after calcination treatments, resulting in a material with high Brønsted acidity, as revealed by NH₃-TPD. The catalytic activity of this nanosized material has been evaluated for the MTO reaction at WHSV = 0.8 h⁻¹ and 350°C, and its catalytic behavior compared with conventional SSZ-13 and SSZ-39 catalysts. The catalyst lifetime of the nanosized SSZ-39 material is remarkably higher than the catalyst lifetime observed for conventional SSZ-13 and SSZ-39 materials.

Acknowledgments

Financial support by the Spanish Government-MINECO through “Severo Ochoa” (SEV 2012-0267), Consolider Ingenio 2010-Multicat, and MAT2012-37160 is acknowledged. The European Union is also acknowledged by the SYNCATMATCH project (Grant

Agreement nº 671093). N. M. thanks MINECO for economical support through pre-doctoral fellowship (BES-2013-064347).

Figure 1: Phase diagrams achieved with the selected OSDAs

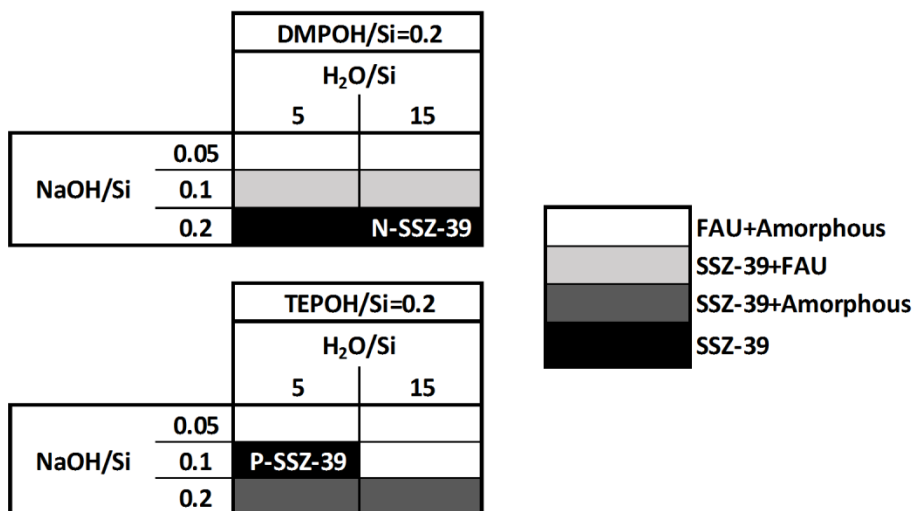


Figure 2: PXRD patterns of the as-synthesized zeolitic materials

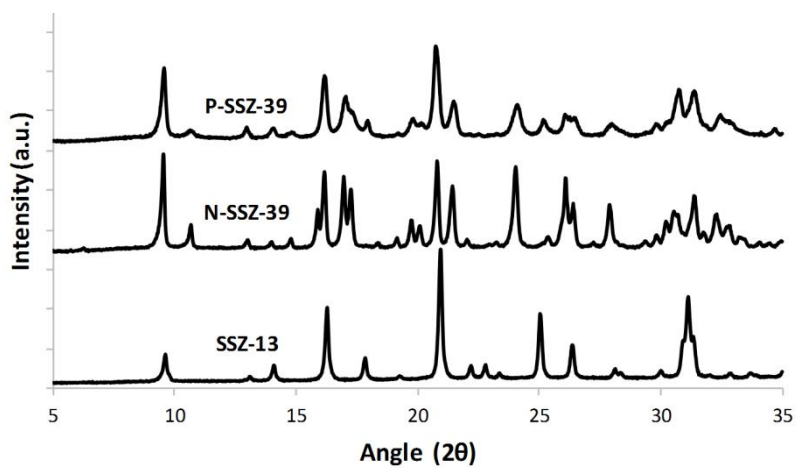


Figure 3: SEM images of the SSZ-13 and SSZ-39 materials

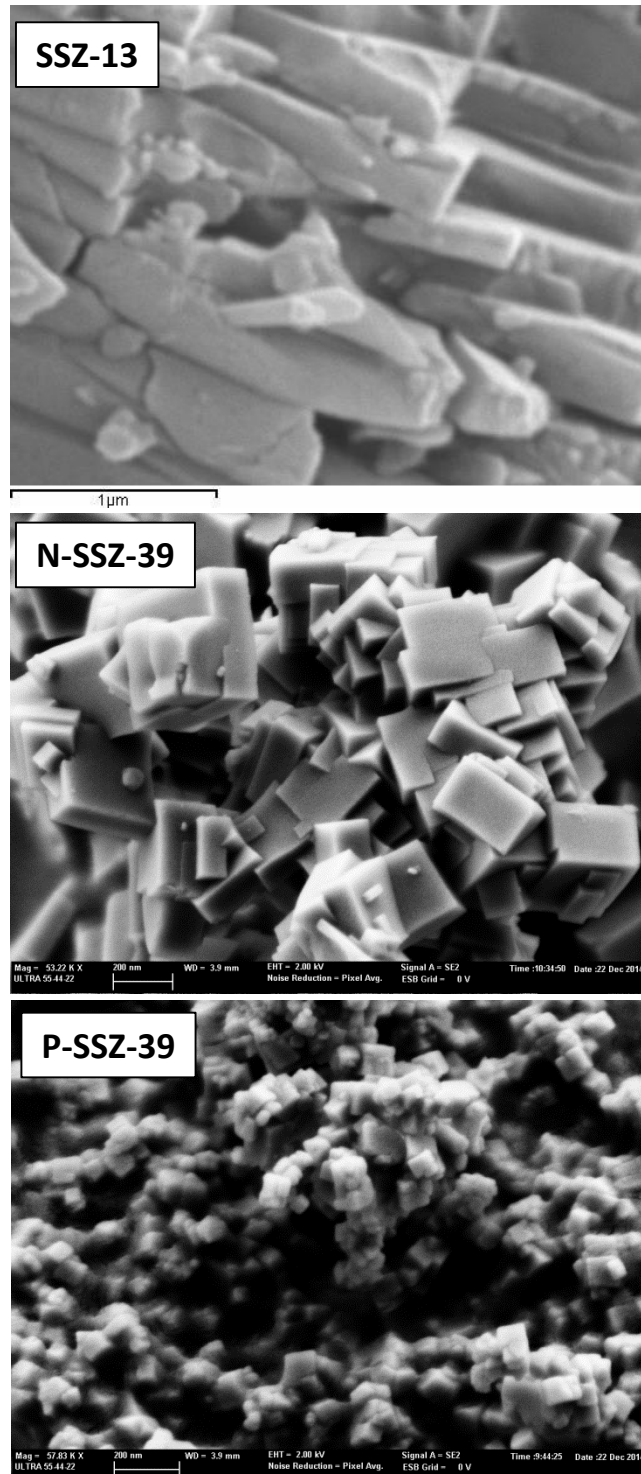


Figure 4: ^{31}P MAS NMR of the as-prepared and calcined P-SSZ-39 materials

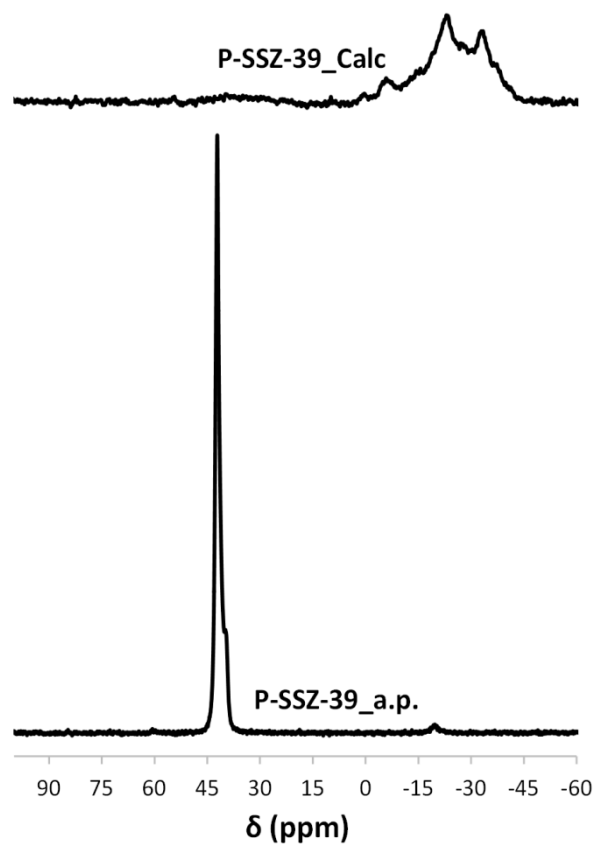


Figure 5: ^{27}Al MAS NMR of the as-prepared and acid SSZ-39 and acid SSZ-13 materials

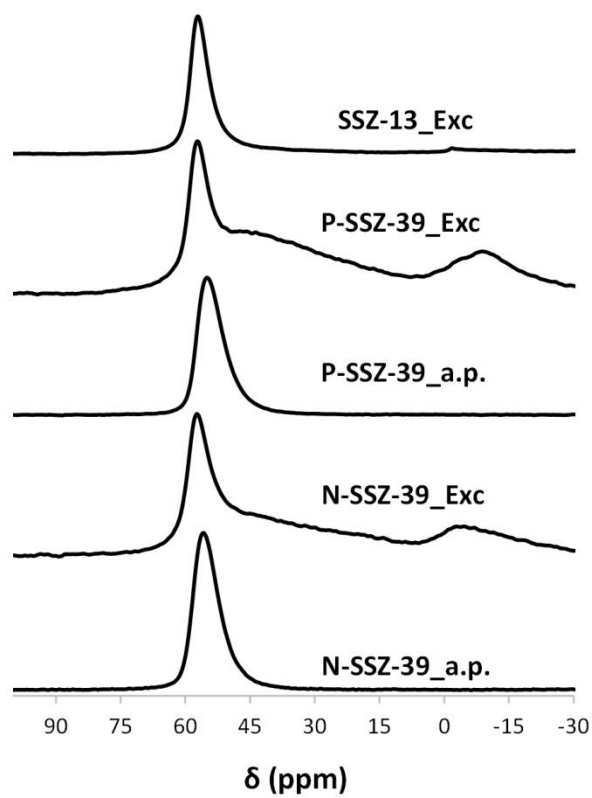


Figure 6: NH₃-TPD profiles of the acid SSZ-13 and SSZ-39 materials

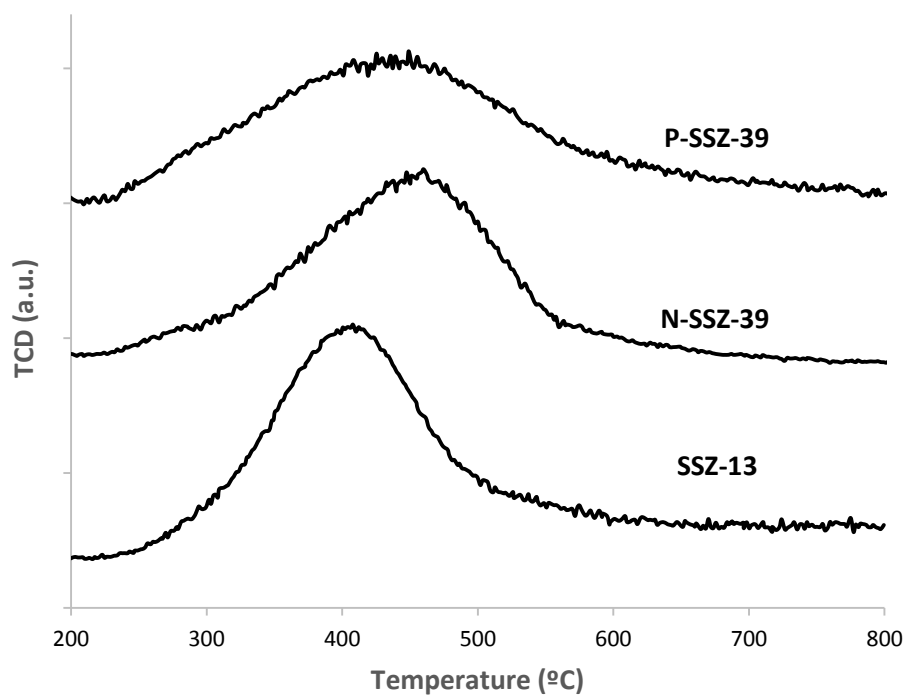


Figure 7: Conversion of methanol at 350°C and $WHSV=0.8h^{-1}$ of the SSZ-13 and SSZ-39 materials (reaction conditions: $T=350^{\circ}C$, 30 ml/min of N_2 bubbled at $-17^{\circ}C$, $WHSV=0.8h^{-1}$, $W_{cat}=50$ mg)

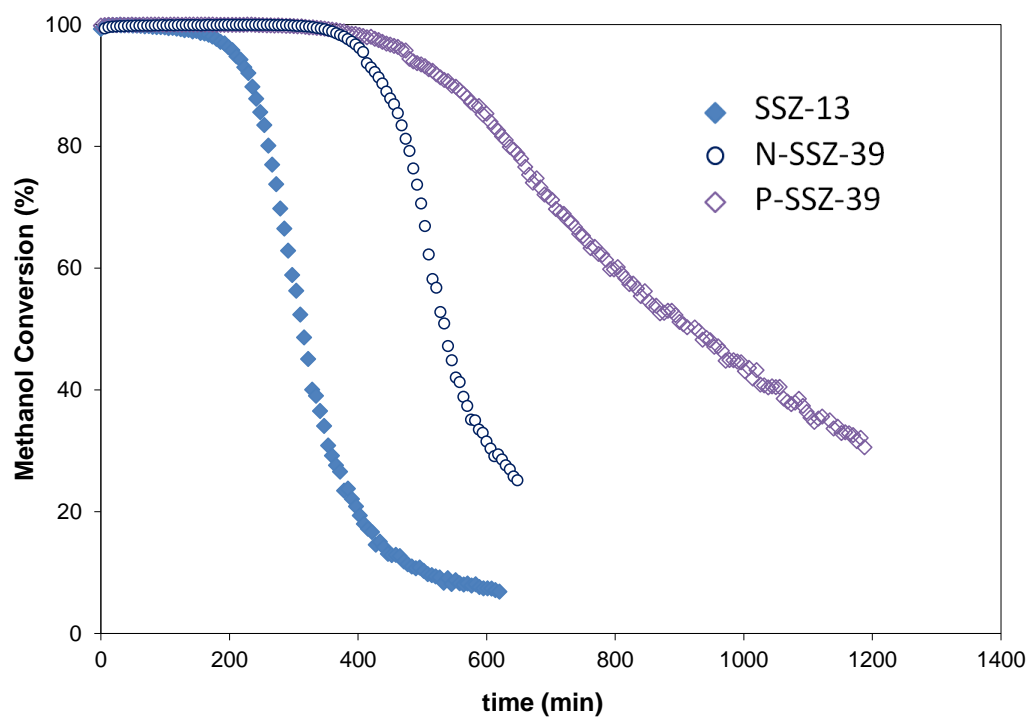


Figure 8: Yields to C2, C3, C4 and C5+ hydrocarbons at different methanol conversions at 350°C and WHSV=0.8 h⁻¹ for the different catalysts.

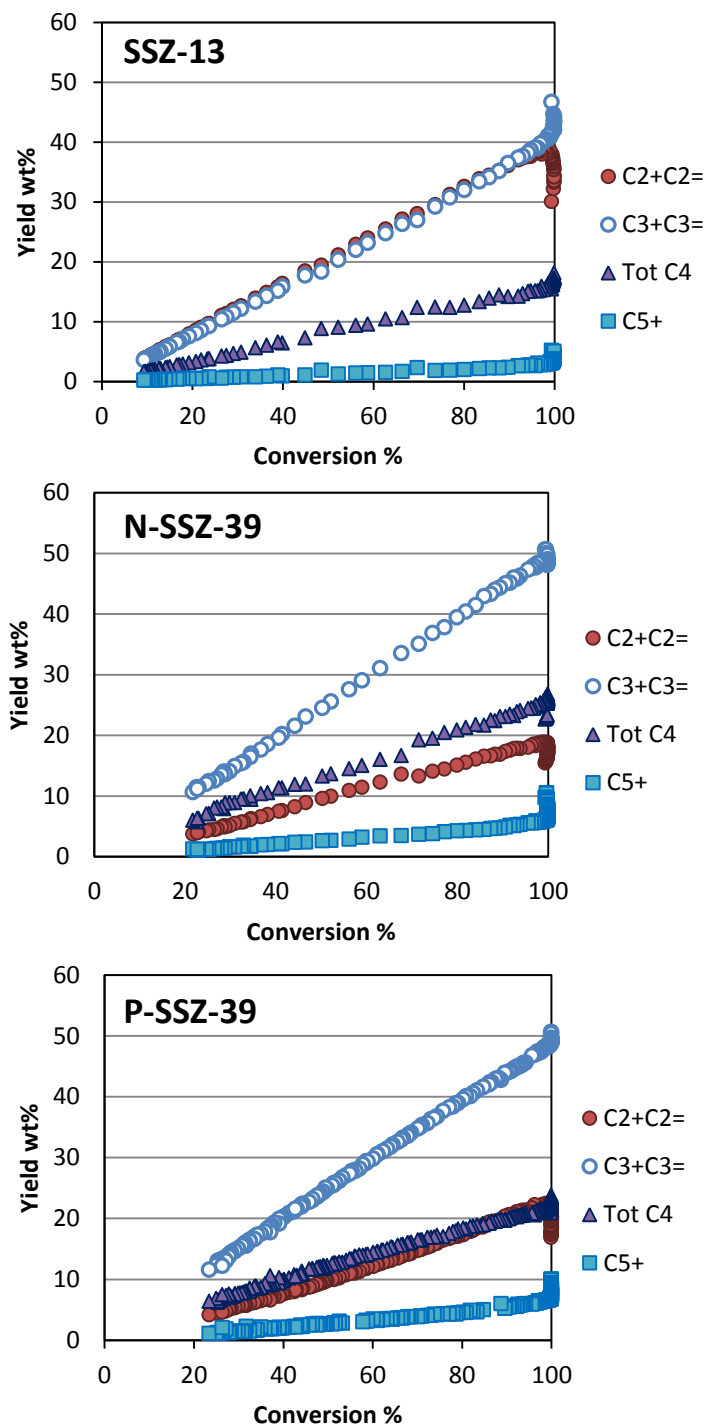


Figure 9: Selectivities to C2, C3, C4 and C5+ hydrocarbons at different methanol conversions for the different catalysts

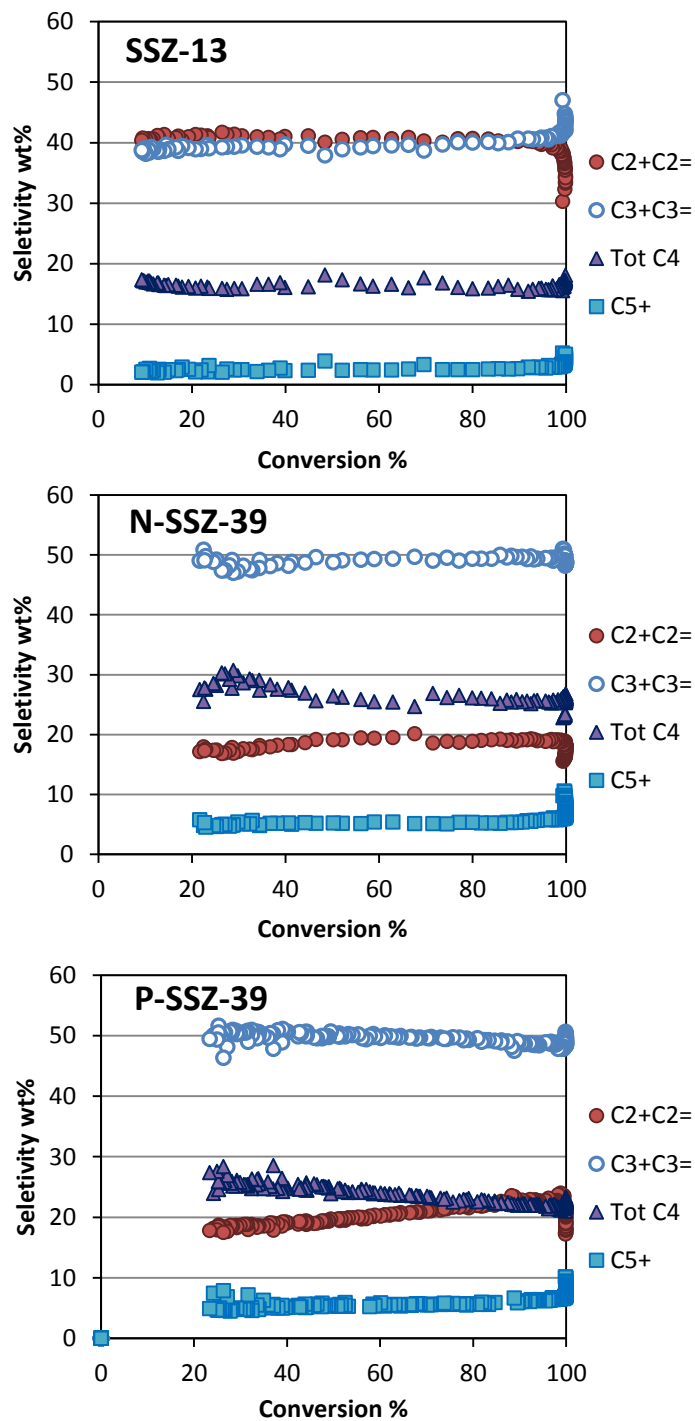


Figure 10: The C2/C3 ratio of the SSZ-13 and SSZ-39 materials in the conversion of methanol at 350°C and WHSV=0.8 h⁻¹.

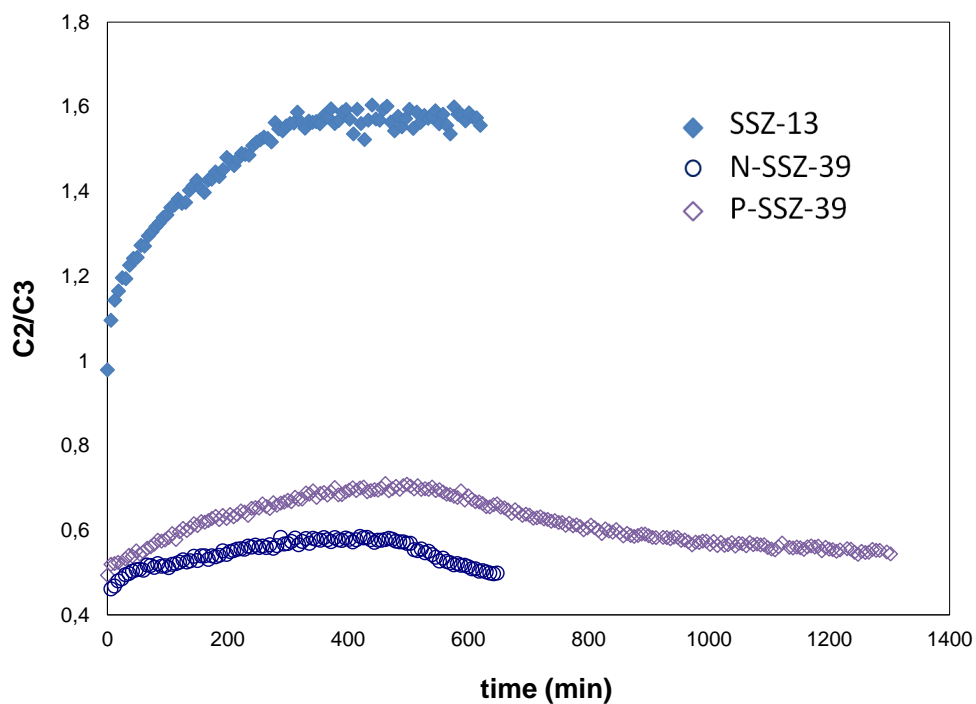


Figure 11: The hydrogen transfer index of the different catalysts against reaction time and methanol conversion

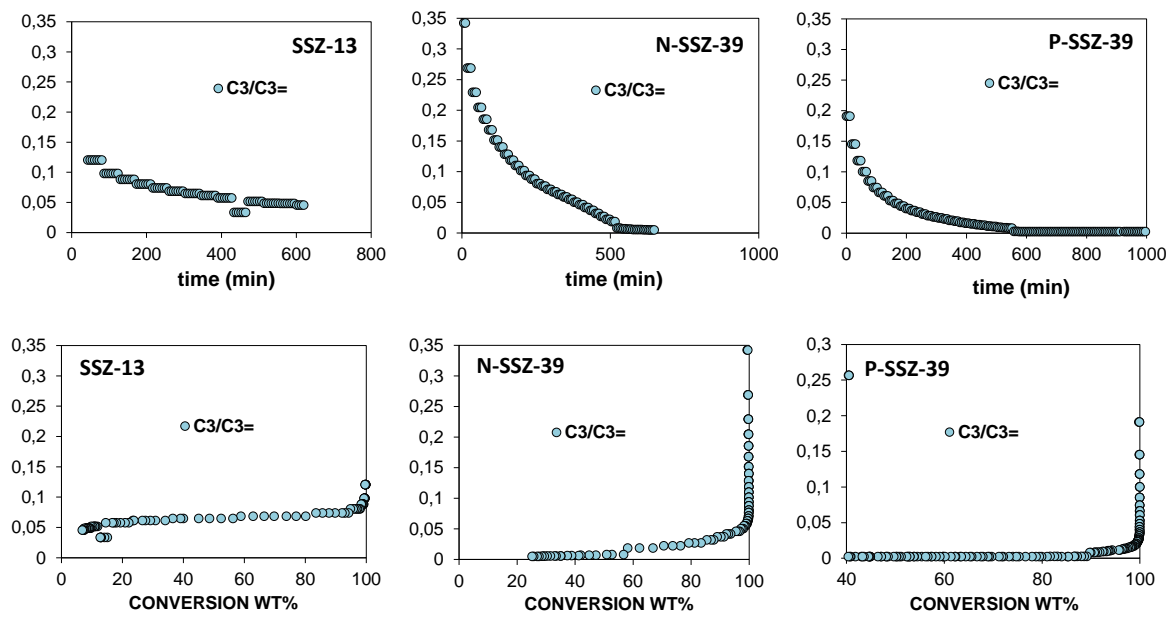


Table 1: Textural properties of the SSZ-13 and SSZ-39 materials.

Sample	Si/Al	OSDA	Crystal size (μm)	BET (m^2/g)	A_{micro} (m^2/g)	A_{Ext} (m^2/g)	V_{micro} (cm^3/g)
SSZ-13	15.3	TMAda	1x0.2	520	517	3	0.25
N-SSZ-39	8.3	DMP	0.2-0.3	516	501	15	0.25
P-SSZ-39	8.5	TPA	0.05	526	484	42	0.23

Table 2: Acidity of the SSZ-13 and SSZ-39 materials measured by adsorption of NH_3 at 175°C

Sample	$\text{NH}_3(\text{mmol/g})$
SSZ-13	0.35
N-SSZ-39	0.54
P-SSZ-39	0.49

References:

- [1] J. Biswas, I.E. Maxwell, Recent process- and catalyst-related developments in fluid catalytic cracking, *Applied Catalysis*, 63 (1990) 197-258.
- [2] P. O'Connor, Chapter 15 Catalytic cracking: The Future of an Evolving Process, in: *Stud. Surf. Sci. Catal.*, 2007, pp. 227-251.
- [3] P. O'Connor, A. Hakuli, P. Imhof, Innovations in producing light olefins by fluid catalytic cracking, *Stud. Surf. Sci. Catal.*, 149 (2004) 305-321.
- [4] Y. Yoshimura, N. Kijima, T. Hayakawa, K. Murata, K. Suzuki, F. Mizukami, K. Matano, T. Konishi, T. Oikawa, M. Saito, T. Shiojima, K. Shiozawa, K. Wakui, G. Sawada, K. Sato, S. Matsuo, N. Yamaoka, Catalytic cracking of naphtha to light olefins, *Catalysis Surveys from Japan*, 4 (2001) 157-167.
- [5] A. Corma, J. Mengual, P.J. Miguel, Steam catalytic cracking of naphtha over ZSM-5 zeolite for production of propene and ethene: Micro and macroscopic implications of the presence of steam, *Applied Catalysis A: General*, 417-418 (2012) 220-235.
- [6] P. Barger, Methanol to olefins (MTO) and beyond, in: M. Guisnet, J.P. Gilson (Eds.) *Zeolites for Cleaner Technologies (Catalytic Science Series Vol. 3)*, Imperial College Press, London, 2002, pp. 239-260.
- [7] P. Tian, Y. Wei, M. Ye, Z. Liu, Methanol to olefins (MTO): From fundamentals to commercialization, *ACS Catalysis*, 5 (2015) 1922-1938.
- [8] M. Moliner, C. Martínez, A. Corma, Synthesis Strategies for Preparing Useful Small Pore Zeolites and Zeotypes for Gas Separations and Catalysis, *Chem. Mater.*, 26 (2014).
- [9] M. Stöcker, Methanol-to-hydrocarbons: Catalytic materials and their behavior, *Microporous Mesoporous Mater.*, 29 (1999) 3-48.
- [10] M. Stöcker, Methanol to Olefins (MTO) and Methanol to Gasoline (MTG), in: *Zeolites and Catalysis*, Wiley-VCH Verlag GmbH & Co. KGaA, 2010, pp. 687-711.
- [11] S. Wilson, P. Barger, The characteristics of SAPO-34 which influence the conversion of methanol to light olefins, *Microporous Mesoporous Mater.*, 29 (1999) 117-126.
- [12] B.P.C. Hereijgers, F. Bleken, M.H. Nilsen, S. Svelle, K.P. Lillerud, M. Bjørgen, B.M. Weckhuysen, U. Olsbye, Product shape selectivity dominates the Methanol-to-Olefins (MTO) reaction over H-SAPO-34 catalysts, *J. Catal.*, 264 (2009) 77-87.
- [13] W. Song, J.F. Haw, J.B. Nicholas, C.S. Heneghan, Methylbenzenes Are the Organic Reaction Centers for Methanol-to-Olefin Catalysis on HSAPO-34, *J. Am. Chem. Soc.*, 122 (2000) 10726-10727.
- [14] D. Chen, K. Moljord, A. Holmen, A methanol to olefins review: Diffusion, coke formation and deactivation on SAPO type catalysts, *Microporous Mesoporous Mater.*, 164 (2012) 239-250.
- [15] S.C. Larsen, Nanocrystalline Zeolites and Zeolite Structures: Synthesis, Characterization, and Applications, *The Journal of Physical Chemistry C*, 111 (2007) 18464-18474.
- [16] T. Tago, H. Konno, Y. Nakasaka, T. Masuda, Size-Controlled Synthesis of Nano-Zeolites and Their Application to Light Olefin Synthesis, *Catal Surv Asia*, 16 (2012) 148-163.
- [17] H. Yang, Z. Liu, H. Gao, Z. Xie, Synthesis and catalytic performances of hierarchical SAPO-34 monolith, *J. Mater. Chem.*, 20 (2010) 3227-3231.
- [18] Y. Li, Y. Huang, J. Guo, M. Zhang, D. Wang, F. Wei, Y. Wang, Hierarchical SAPO-34/18 zeolite with low acid site density for converting methanol to olefins, *Catal. Today*, 233 (2014) 2-7.
- [19] F. Schmidt, S. Paasch, E. Brunner, S. Kaskel, Carbon templated SAPO-34 with improved adsorption kinetics and catalytic performance in the MTO-reaction, *Microporous Mesoporous Mater.*, 164 (2012) 214-221.
- [20] Q. Sun, N. Wang, G. Guo, X. Chen, J. Yu, Synthesis of tri-level hierarchical SAPO-34 zeolite with intracrystalline micro-meso-macroporosity showing superior MTO performance, *Journal of Materials Chemistry A*, 3 (2015) 19783-19789.

- [21] Q. Sun, N. Wang, D. Xi, M. Yang, J. Yu, Organosilane surfactant-directed synthesis of hierarchical porous SAPO-34 catalysts with excellent MTO performance, *Chem. Commun.*, 50 (2014) 6502-6505.
- [22] C. Wang, M. Yang, P. Tian, S. Xu, Y. Yang, D. Wang, Y. Yuan, Z. Liu, Dual template-directed synthesis of SAPO-34 nanosheet assemblies with improved stability in the methanol to olefins reaction, *Journal of Materials Chemistry A*, 3 (2015) 5608-5616.
- [23] S.T. Yang, J.Y. Kim, H.J. Chae, M. Kim, S.Y. Jeong, W.S. Ahn, Microwave synthesis of mesoporous SAPO-34 with a hierarchical pore structure, *Mater. Res. Bull.*, 47 (2012) 3888-3892.
- [24] Q. Sun, N. Wang, G. Guo, J. Yu, Ultrafast synthesis of nano-sized zeolite SAPO-34 with excellent MTO catalytic performance, *Chem. Commun.*, (2015).
- [25] G. Yang, Y. Wei, S. Xu, J. Chen, J. Li, Z. Liu, J. Yu, R. Xu, Nanosize-Enhanced Lifetime of SAPO-34 Catalysts in Methanol-to-Olefin Reactions, *The Journal of Physical Chemistry C*, 117 (2013) 8214-8222.
- [26] Z. Li, J. Martínez-Triguero, P. Concepcion, J. Yu, A. Corma, Methanol to olefins: activity and stability of nanosized SAPO-34 molecular sieves and control of selectivity by silicon distribution, *PCCP*, 15 (2013) 14670-14680.
- [27] L.T. Yuen, S.I. Zones, T.V. Harris, E.J. Gallegos, A. Auroux, Product selectivity in methanol to hydrocarbon conversion for isostructural compositions of AFI and CHA molecular sieves, *Microporous Mater.*, 2 (1994) 105-117.
- [28] F. Bleken, M. Bjørgen, L. Palumbo, S. Bordiga, S. Svelle, K.P. Lillerud, U. Olsbye, The effect of acid strength on the conversion of methanol to olefins over acidic microporous catalysts with the CHA topology, *Top. Catal.*, 52 (2009) 218-228.
- [29] Q. Zhu, J.N. Kondo, R. Ohnuma, Y. Kubota, M. Yamaguchi, T. Tatsumi, The study of methanol-to-olefin over proton type aluminosilicate CHA zeolites, *Microporous Mesoporous Mater.*, 112 (2008) 153-161.
- [30] Y. Bhawe, M. Moliner-Marin, J.D. Lunn, Y. Liu, A. Malek, M. Davis, Effect of cage size on the selective conversion of methanol to light olefins, *ACS Catalysis*, 2 (2012) 2490-2495.
- [31] L. Wu, V. Degirmenci, P.C.M.M. Magusin, N.J.H.G.M. Lousberg, E.J.M. Hensen, Mesoporous SSZ-13 zeolite prepared by a dual-template method with improved performance in the methanol-to-olefins reaction, *J. Catal.*, 298 (2013) 27-40.
- [32] Y. Ji, M.A. Deimund, Y. Bhawe, M.E. Davis, Organic-Free Synthesis of CHA-Type Zeolite Catalysts for the Methanol-to-Olefins Reaction, *ACS Catalysis*, 5 (2015) 4456-4465.
- [33] Z. Li, J. Martínez-Triguero, J. Yu, A. Corma, Conversion of methanol to olefins: Stabilization of nanosized SAPO-34 by hydrothermal treatment, *J. Catal.*, 329 (2015) 379-388.
- [34] J. Wang, D. Fan, T. Yu, J. Wang, T. Hao, X. Hu, M. Shen, W. Li, Improvement of low-temperature hydrothermal stability of Cu/SAPO-34 catalysts by Cu²⁺ species, *J. Catal.*, 322 (2015) 84-90.
- [35] S.I. Zones, Y. Nakagawa, S.T. Evans, G.S. Lee, Synthesis, properties, and applications of small-pore zeolite SSZ-39 for use as petroleum refining catalysts, US5958370A (1999), to Chevron U.S.A. Inc., USA .
- [36] P. Wagner, Y. Nakagawa, G.S. Lee, M.E. Davis, S. Elomari, R.C. Medrud, S.I. Zones, Guest/Host Relationships in the Synthesis of the Novel Cage-Based Zeolites SSZ-35, SSZ-36, and SSZ-39, *J. Am. Chem. Soc.*, 122 (2000) 263-273.
- [37] M. Dusselier, M.A. Deimund, J.E. Schmidt, M.E. Davis, Methanol-to-Olefins Catalysis with Hydrothermally Treated Zeolite SSZ-39, *ACS Catalysis*, 5 (2015) 6078-6085.
- [38] M. Moliner, C. Franch, E. Palomares, M. Grill, A. Corma, Cu-SSZ-39, an active and hydrothermally stable catalyst for the selective catalytic reduction of NO_x, *Chem. Commun.*, 48 (2012) 8264-8266.
- [39] M. Dusselier, J.E. Schmidt, R. Moulton, B. Haymore, M. Hellums, M.E. Davis, Influence of Organic Structure Directing Agent Isomer Distribution on the Synthesis of SSZ-39, *Chem. Mater.*, 27 (2015) 2695-2702.

- [40] T. Maruo, N. Yamanaka, N. Tsunoji, M. Sadakane, T. Sano, Facile synthesis of AEI zeolites by hydrothermal conversion of FAU zeolites in the presence of tetraethylphosphonium cations, *Chem. Lett.*, 43 (2014) 302-304.
- [41] T. Sonoda, T. Maruo, Y. Yamasaki, N. Tsunoji, Y. Takamitsu, M. Sadakane, T. Sano, Synthesis of high-silica AEI zeolites with enhanced thermal stability by hydrothermal conversion of FAU zeolites, and their activity in the selective catalytic reduction of NO_x with NH₃, *Journal of Materials Chemistry A*, 3 (2015) 857-865.
- [42] N. Martin, C.R. Boruntea, M. Moliner, A. Corma, Efficient synthesis of the Cu-SSZ-39 catalyst for DeNO_x applications, *Chem. Commun.*, 51 (2015) 11030-11033.
- [43] L. Tosheva, V.P. Valtchev, Nanozeolites: Synthesis, Crystallization Mechanism, and Applications, *Chem. Mater.*, 17 (2005) 2494-2513.
- [44] M. Moliner, F. Rey, A. Corma, Towards the rational design of efficient organic structure-directing agents for zeolite synthesis, *Angewandte Chemie - International Edition*, 52 (2013) 13880-13889.
- [45] S.I. Zones, Zeolite SSZ-13, 4544538, to
- [46] F.L. Bleken, T.V.W. Janssens, S. Svelle, U. Olsbye, Product yield in methanol conversion over ZSM-5 is predominantly independent of coke content, *Microporous Mesoporous Mater.*, 164 (2012) 190-198.
- [47] W. Skistad, S. Teketel, F.L. Bleken, P. Beato, S. Bordiga, M.H. Nilsen, U. Olsbye, S. Svelle, K.P. Lillerud, Methanol conversion to hydrocarbons (MTH) over H-ITQ-13 (ITH) zeolite, *Top. Catal.*, 57 (2014) 143-158.
- [48] T. Álvaro-Muñoz, C. Márquez-Álvarez, E. Sastre, Mesopore-Modified SAPO-18 with Potential Use as Catalyst for the MTO Reaction, *Top. Catal.*, (2015) 1-14.
- [49] R.L. Smith, S. Svelle, P. del Campo, T. Fuglerud, B. Arstad, A. Lind, S. Chavan, M.P. Atfield, D. Akporiaye, M.W. Anderson, CHA/AEI intergrowth materials as catalysts for the Methanol-to-Olefins process, *Applied Catalysis A: General*, 505 (2015) 1-7.
- [50] J. Chen, J. Li, Y. Wei, C. Yuan, B. Li, S. Xu, Y. Zhou, J. Wang, M. Zhang, Z. Liu, Spatial confinement effects of cage-type SAPO molecular sieves on product distribution and coke formation in methanol-to-olefin reaction, *Catal. Commun.*, 46 (2014) 36-40.
- [51] T. Yokoi, M. Yoshioka, H. Imai, T. Tatsumi, Diversification of RTH-type zeolite and its catalytic application, *Angewandte Chemie - International Edition*, 48 (2009) 9884-9887+9767.
- [52] A. Ghysels, S.L.C. Moors, K. Hemelsoet, K. De Wispelaere, M. Waroquier, G. Sastre, V. Van Speybroeck, Shape-Selective Diffusion of Olefins in 8-Ring Solid Acid Microporous Zeolites, *The Journal of Physical Chemistry C*, 119 (2015) 23721-23734.
- [53] N. Hedin, G.J. DeMartin, W.J. Roth, K.G. Strohmaier, S.C. Reyes, PFG NMR self-diffusion of small hydrocarbons in high silica DDR, CHA and LTA structures, *Microporous Mesoporous Mater.*, 109 (2008) 327-334.
- [54] C.D. Chang, C.T.W. Chu, R.F. Socha, Methanol conversion to olefins over ZSM-5: I. Effect of temperature and zeolite SiO₂/Al₂O₃, *J. Catal.*, 86 (1984) 289-296.
- [55] M. Bjorgen, S. Svelle, F. Joensen, J. Nerlov, S. Kolboe, F. Bonino, L. Palumbo, S. Bordiga, U. Olsbye, Conversion of methanol to hydrocarbons over zeolite H-ZSM-5: On the origin of the olefinic species, *J. Catal.*, 249 (2007) 195-207.
- [56] C.-J. Chen, S. Rangarajan, I.M. Hill, A. Bhan, Kinetics and Thermochemistry of C₄-C₆ Olefin Cracking on H-ZSM-5, *ACS Catalysis*, 4 (2014) 2319-2327.
- [57] W. Dai, C. Wang, M. Dyballa, G. Wu, N. Guan, L. Li, Z. Xie, M. Hunger, Understanding the Early Stages of the Methanol-to-Olefin Conversion on H-SAPO-34, *ACS Catalysis*, 5 (2015) 317-326.
- [58] C.-M. Wang, Y.-D. Wang, Y.-J. Du, G. Yang, Z.-K. Xie, Similarities and differences between aromatic-based and olefin-based cycles in H-SAPO-34 and H-SSZ-13 for methanol-to-olefins conversion: insights from energetic span model, *Catalysis Science & Technology*, 5 (2015) 4354-4364.

[59] K. De Wispelaere, K. Hemelsoet, M. Waroquier, V. Van Speybroeck, Complete low-barrier side-chain route for olefin formation during methanol conversion in H-SAPO-34, *J. Catal.*, 305 (2013) 76-80.

[60] C.-M. Wang, Y.-D. Wang, H.-X. Liu, G. Yang, Y.-J. Du, Z.-K. Xie, Aromatic-based hydrocarbon pool mechanism for methanol-to-olefins conversion in H-SAPO-18: A van der Waals density functional study, *Chinese Journal of Catalysis*, 36 (2015) 1573-1579.